



Evaluating the correlation of the impairment between skeletal muscle and heart using MRI in a spontaneous type 2 diabetes mellitus rhesus monkey model

Yushu Chen¹ · Wen Zeng² · Wei Chen^{1,3} · Yu Zhang¹ · Tong Zhu¹ · Jiayu Sun¹ · Zhigang Liang² · Lei Wang¹ · Zunyuan Yang² · Bing Wu¹ · Bin Song¹ · Fangtong Wang² · Yinan Liang² · Li Gong² · Jie Zheng⁴ · Fabao Gao^{1,2} 

Received: 27 September 2019 / Accepted: 20 November 2019 / Published online: 14 January 2020
© Springer-Verlag Italia S.r.l., part of Springer Nature 2020

Abstract

Aims To investigate the correlation of impairment in skeletal muscle and heart in spontaneous type 2 diabetes mellitus (T2DM) rhesus monkeys using magnetic resonance image (MRI).

Methods Fifteen T2DM monkeys and fourteen healthy control (HC) monkeys were included. The microcirculation of skeletal muscle [skeletal muscle blood flow (SMBF), skeletal muscle oxygen extraction fraction (SMOEF)] and the function and strain of heart were evaluated by MRI. Three regions of interests were chosen on the soleus muscle (SOL), gastrocnemius muscle (GAS) and tibialis anterior muscle (TA) for image analysis.

Results Eight T2DM monkeys and eight HC monkeys were obtained the full data. The SMBF reserves and SMOEF reserves were found significantly decreased in T2DM during inflation in SOL, GAS and TA muscles (all $p < 0.05$), and the SMBF reserves decreased during hyperemia in GAS and TA muscles (all $p < 0.05$). In these monkeys, the global peak longitudinal strain (longitudinal PS), peak systolic longitudinal strain rate (longitudinal PSSR) and peak diastolic longitudinal strain rate (longitudinal PDSR) were seen significantly different in T2DM compared to HC monkeys (all $p < 0.05$). The longitudinal PSSR was found negatively correlated with SMBF reserves in SOL, GAS and TA during inflation in all monkeys.

Conclusions The impaired microcirculation of skeletal muscle and the myocardial deformation were found in T2DM monkeys with normal ejection fraction. And a negative correlation was existed in the longitudinal PSSR and the SMBF reserves.

Keywords Diabetes · Impairment · Microcirculation · MRI · Monkey

Introduction

Type 2 diabetes mellitus (T2DM) is associated with long-term damage and dysfunction of vessels and cells [1], affecting the skeletal muscle and myocardium, leading to the

development of diabetic lower extremities and diabetic cardiomyopathy and then resulted in the amputation and heart failure [2, 3]. It is reported that one of four patients with diabetic wounds had an amputation [4], and 30.9 per 1000 person diabetic patients had heart failure [5]. The insidious onset, the delayed diagnosis, treatment difficult and poor prognosis of the complications are all of the reasons [5, 6]. In previous studies, much evidence points toward the chronic heart failure accompanied with the skeletal muscle alterations [7–9]. Therefore, gaining an insight into the impairments of skeletal muscle and cardiac muscle and finding the correlations of these impairments may play an important role in early diagnosis of the complications of T2DM, and outcomes prediction. However, in our knowledge, there are few noninvasive image studies to explore whether there are the correlations between the impairments of skeletal muscle and cardiac muscle.

Managed By Antonio Secchi.

✉ Fabao Gao
gaofabao@wchscu.cn

¹ Department of Radiology, Sichuan University West China Hospital, 37 Guoxuexiang, Chengdu 610041, Sichuan, China

² Sichuan Primed Shines Biotech Co., Ltd., Chengdu, China

³ Department of Radiology, First Affiliated Hospital of Kunming Medical University, Kunming, China

⁴ Mallinckrodt Institute of Radiology, Washington University School of Medicine, St. Louis, MO, USA

Magnetic resonance image (MRI) is a powerful visualization method that provides the unique capability to not only detect the organic dysfunction, but also quantitatively characterize examined tissue [10]. Lots of studies have explored the changes of heart in T2DM in both human and animals [10–12]. The perfusion and oxygenation MR techniques were attempted in limited volunteers and patients mixed Type 1 and T2DM [13–15], as well. In this study, considering the complicated diabetes duration, individual medical history in patients and the huge value of spontaneous T2DM monkeys in investigating the basis of complications arising from T2DM, efficacy of diagnosis and treatments as well as drug development [16, 17], the study evaluated the function and strain of the heart and the microcirculation of skeletal muscle in spontaneous T2DM rhesus monkeys to characterize the impaired skeletal muscle and heart, and then to investigate the relationship for different sites (skeletal muscle and heart) in T2DM.

Materials and methods

Animals

Fifteen spontaneous T2DM rhesus monkeys and fourteen age-matched, healthy control (HC) monkeys with well-controlled glucose level were included. The criteria used for the monkey selections were guided by previous works [12, 18], and none of the monkeys had a history of medical treatment. The animals had ad libitum access to a standard monkey diet (calories provided from protein, 17%; from fat, 30%; and from carbohydrates, 53%).

MRI

All monkeys underwent 3.0T clinical MRI (Magnetom Trio; Siemens Healthcare, Malvern, Pa) with a 32-channel cardiac coil and a surface soft coil for leg. An air cuff was placed on the mid-thigh above the right knee to provoke ischemic/reperfusion of skeletal muscle. Ischemia was achieved by using manual inflation of the cuff to an occlusion pressure of 45 mmHg above the individual branchial systolic blood pressure. The MRI surface coil was covered over the calf. Three slices including the largest cross section in the calf were chosen to image. An arterial spin-labeling (ASL) method was adapted for the skeletal muscle blood flow (SMBF) using the following parameters: gradient-echo acquisition; repetition time (TR)=2.8 ms, echo time (TE)=1.2 ms; 10 T1-weighted images (T1WI) for each T1 measurement; flip angle=5°; field of view (FOV)=160×112 mm²; slice thickness=8 mm; data acquisition matrix=128×90; data average=3; acquisition time=60 s. There were a total of 12 SMBF measurements for 1 min per time point. The

MRI method for skeletal muscle oxygen extraction fraction (SMOEF) measurement was employed to acquire multiple T1WI for SMOEF measurements at the same slice location as the ASL measurements. The imaging parameters are: TR=4 s; TE1/TE2/TE3=44/62/80 ms; FOV=160×140 mm²; matrix size=64×56 and interpolated to 128×112; and single slice thickness=8 mm. The SMOEF scan lasted for 4 min, yielding a rate of SMOEF imaging of 4 min per time point, for a total of 3 SMOEF measurements. For cardiac MRI, the imaging protocols consisted of balanced steady-state free precession retrospective electrocardiographically gated (ECG-gated) breath-hold sequences acquired in expiration in the two-chamber, four-chamber views and short-axis images with the following sequence parameters: TR=16.85 ms, TE=1.44 ms, FOV=136×160 mm², slice thickness=6 mm, phases=25. Late gadolinium enhancement (LGE) images were obtained using ECG-gated breath-hold inversion recovery Turbo FLASH sequence in three short-axis slices at the base, middle and apex of the left ventricle (LV), and in two-chamber, four-chamber views. The MRI scan interval between heart and leg was not more than 24 h. Details of the image scheme are seen in Fig. 1.

Image analysis

SMBF and SMOEF

SMBF maps and SMOEF maps were created using custom-made software written in MATLAB (MathWorks, Natick, MA) according the previous studies [15] by two radiologists (C.Y.S. and G.F.B.) with 6 years and 15 years of experience, respectively, in radiology diagnosis and an MRI specialist (Z.J.) with 20 years of image analysis. Three ROIs (soleus muscle, SOL; gastrocnemius muscle, GAS; and tibialis anterior muscle, TA) were selected as shown in Fig. 1. The resting and inflation SMBF were averaged over four measurements (4 min), and hyperemia SMBF was averaged over two measurements immediately after cuff deflation since the hyperemia period last approximately 2 min, according to the previous studies [19]. All SMBF and SMOEF were normalized by respective resting SMBF and SMOEF for the SMBF reserves and SMOEF reserves.

Function and strain characteristics

LV volumes, function, strain and tissue characteristics were performed offline with cmr⁴² software (Circle Cardiovascular Imaging, Calgary, Canada) by three radiologists (C.W., Z.Y. and Z.T.) with 10 years and 3 years of experience in cardiac MRI diagnosis. Global strains were analyzed as follows: the global peak radial strain (radial PS), the global peak circumferential strain (circumferential PS), global

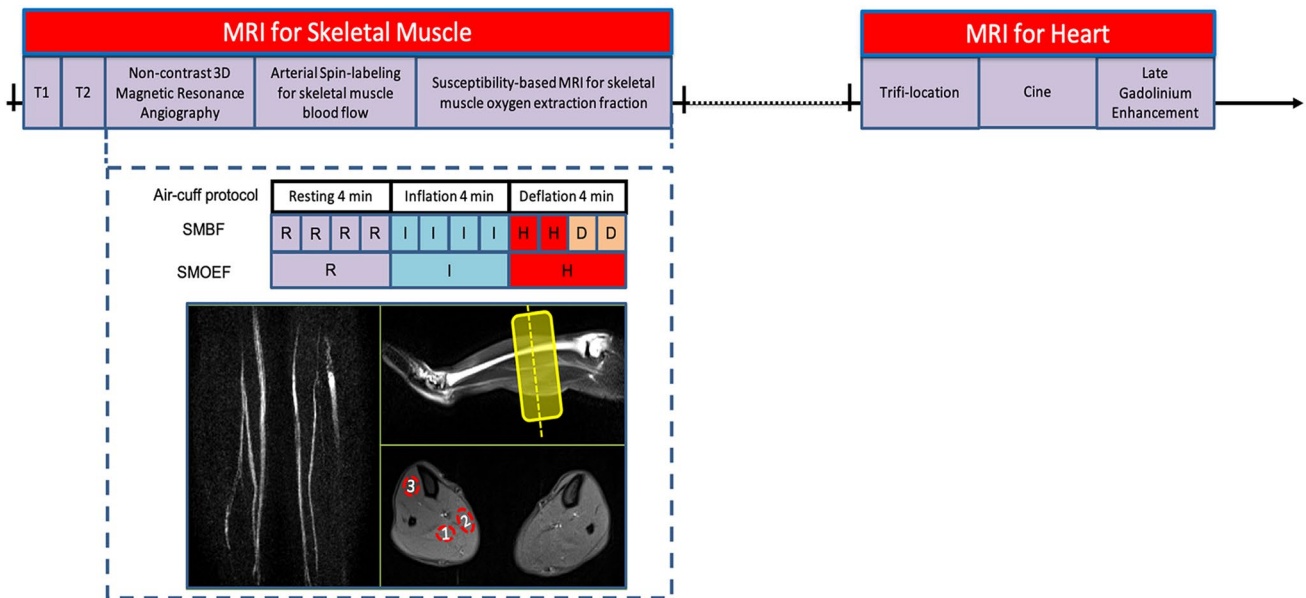


Fig. 1 MRI scheme. All rhesus monkeys were scanned by MRI as the imaging scheme. *R* resting, *I* inflation, *H* hyperemia, *D* deflation, *ROI 1* soleus muscle, *ROI 2* gastrocnemius muscle, *ROI 3* tibialis anterior muscle

peak longitudinal strain (longitudinal PS), peak systolic radial strain rate (radial PSSR), peak systolic circumferential strain rate (circumferential PSSR), peak systolic longitudinal strain rate (longitudinal PSSR), peak diastolic radial strain rate (radial PDSR), peak diastolic circumferential strain rate (circumferential PDSR), peak diastolic longitudinal strain rate (longitudinal PDSR), peak torsion ($^{\circ}$) and peak torsion rate ($^{\circ}/s$).

Histology

Two T2DM monkeys were killed after MRI scanning, and the histologic slices from the myocardium and skeletal muscle were harvested, fixed in methanol and embedded in paraffin. After dehydration and embedding, the slices were subjected to the Masson staining, hematoxylin and eosin (HE) staining and CD31 staining using anti-CD31 polyclonal antibody (Abcam Singapore Pte., Ltd.) according to standard protocols and analyzed under a light microscope (DM500; Leica, Wetzlar, Germany) by a pathologist (T.C.) with 7 years of experience in pathology, blinded to the MR images.

Statistical analysis

Statistical analysis was performed using SPSS 19.0 software (SPSS Inc., Chicago, IL, USA) and Prism 6 (GraphPad Software Inc., La Jolla, California). Data are reported as mean \pm standard deviation. The comparison between the HC and T2DM groups was made using independent

samples T tests. The comparisons among resting, inflation and reactive hyperemia, as well as among different muscle compartments, were determined by one-way analysis of variance (ANOVA) and following post hoc as appropriate. The correlations between cardiac MR parameters and SMBF or SMOEF were assessed using Pearson's correlation analysis or Spearman method. For all comparisons, $p < 0.05$ was considered statistically significant.

Results

Eight T2DM monkeys and eight HC monkeys were finally used for analysis due to the motion artifacts, arrhythmia in the heart or the metal artifacts in the leg in the other monkeys. The general information of the 16 monkeys is seen in Table 1. No difference was found in age and body weight. The mean diabetes duration was 2.43 ± 1.18 years. The fasting plasma glucose (FPG, 7.16 ± 1.46 vs. 4.48 ± 0.30 mmol/L, $p < 0.01$) and glycated hemoglobin (HbA1c, 6.1 ± 1.95 vs. 4.09 ± 0.06 , $p < 0.05$) were higher in T2DM monkeys. No difference was found with regard to total cholesterol, triglycerides, low-density lipoprotein and high-density lipoprotein.

Microcirculation characteristics in skeletal muscle

As shown in Fig. 2, there were significant decreases in SMBF reserves (T2DM vs. HC: 0.98 ± 0.34 vs. 1.38 ± 0.18 in SOL, $p < 0.04$; 0.74 ± 0.32 vs. 1.14 ± 0.19 in GAS, $p < 0.03$; 0.71 ± 0.27 vs. 1.15 ± 0.20 in TA, $p = 0.01$) and in SMOEF

Table 1 Baseline characteristics of study subjects

Characteristic	T2DM	HC	<i>p</i> value
Number (<i>n</i>)	8	8	
Male sex	7 (1)	8	
Mean age (years)	13.54 ± 1.66	13.87 ± 0.74	NS
Mean body weight (kg)	10.31 ± 1.99	11.23 ± 1.28	NS
Mean diabetes duration (years)	2.43 ± 1.10	0	< 0.01
FPG (mmol/l)	7.16 ± 1.46	4.48 ± 0.30	< 0.01
HbA1c (%)	6.1 ± 1.95	4.09 ± 0.06	< 0.05
TC (mmol/l)	3.25 ± 0.43	2.99 ± 0.58	NS
TG (mmol/l)	0.67 ± 0.32	0.43 ± 0.10	NS
LDL (mmol/l)	1.38 ± 0.43	1.21 ± 0.17	NS
HDL (mmol/l)	1.43 ± 0.38	1.86 ± 0.59	NS

Data given as mean ± standard deviation or *n*. Statistical significance was set at *p* < 0.05

FPG fasting plasma glucose, HbA1c glycated hemoglobin, HDL serum high-density lipoprotein, LDL serum low-density lipoprotein, T2DM type 2 diabetes mellitus, TC serum total cholesterol, TG serum triglyceride

reserves (T2DM vs. HC: 1.17 ± 0.04 vs. 1.41 ± 0.17 in SOL, *p* < 0.02; 1.05 ± 0.08 vs. 1.41 ± 0.16 in GAS, *p* < 0.001; 1.12 ± 0.13 vs. 1.32 ± 0.08 in TA, *p* < 0.02) in all muscles during the inflation phase when compared T2DM to HC. The SMBF reserves also decreased during the hyperemia phase in both GAS and TA (T2DM vs. HC: 1.18 ± 0.30 vs. 1.64 ± 0.28 in GAS, *p* < 0.03; 1.19 ± 0.34 vs. 1.63 ± 0.15 in TA, *p* < 0.03). Within T2DM or HC group, the SMBF reserve during the hyperemia was significantly higher in the SOL than that in the GAS or TA (Fig. 2). But for the SMBF and SMOEF, there is no significant difference between T2DM and HC groups in all muscles during each phase, except SMBF in GAS at resting phase and SMOEF in SOL and GAS at resting phase (Table 2).

Myocardial deformation

Table 3 presented the baseline cardiac MRI characteristics of the monkeys with T2DM and HC groups. No significant difference was observed in the ejection fraction (66.8 ± 7.81% vs. 67.5 ± 7.83%, *p* = 0.58), as well as end-diastolic volume index, end-systolic volume index, stroke volume and cardiac output. LGE were negative in both groups. The myocardial strain assessment revealed the significant differences in the longitudinal PS (−9.55 ± 2.77 vs. −13.59 ± 1.97, *p* < 0.05), longitudinal PSSR (−1.00 ± 0.31 vs. −1.51 ± 0.38, *p* < 0.05) and longitudinal PDSR (0.91 ± 0.20 vs. 1.36 ± 0.23, *p* < 0.05) between T2DM and HC. No significant differences were seen in other strain parameters in this study (Table 3).

Correlation between microcirculation of skeletal muscle and myocardial strain

Longitudinal PSSR had negative correlation with SMBF reserves in SOL (*r* = −0.672, *p* = 0.004), in GAS (*r* = −0.577, *p* = 0.019) and in TA (*r* = −0.607, *p* = 0.013) during inflation stage (Fig. 2) in all monkeys.

Histology

The vacuoles in myocytes, perivascular and interstitial fibrosis, and inflammatory cell infiltration were confirmed in heart in the two T2DM monkeys. Myocytolysis and vacuoles were also present in skeletal muscle, accompanied by nuclear translocation. The number of muscle capillaries (CD31-positive vessel) in the skeletal muscle was sparse and different to the myocardium (Fig. 3).

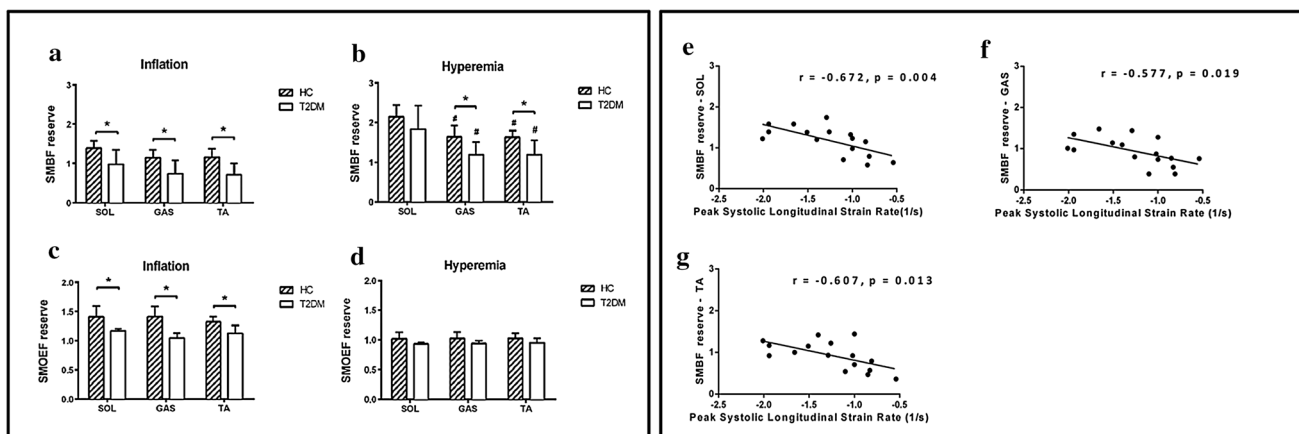


Fig. 2 The changes of SMBF reserves and SMOEF reserves between T2DM and HC, and their relationships with the longitudinal PSSR. **a**, **c** The changes of SMBF reserves and SMOEF reserves during inflation stage among SOL, GAS and TA between T2DM and HC; **b**, **d**

the changes of SMBF reserves and SMOEF reserves during hyperemia stage among SOL, GAS and TA between T2DM and HC. **e–g** Negative correlations between the longitudinal PSSR and the SMBF reserves in SOL, GAS and TA during inflation stage, respectively

Table 2 The dynamic changes of the absolute SMBF and SMOEF values

	Resting			Inflation			Hyperemia		
	SOL	GAS	TA	SOL	GAS	TA	SOL	GAS	TA
SMBF									
HC	0.10±0.05	0.10±0.03	0.14±0.09	0.14±0.06	0.12±0.03	0.15±0.08	0.21±0.10	0.16±0.03	0.23±0.15
T2DM	0.13±0.03	0.15±0.03*	0.17±0.06	0.12±0.04	0.11±0.04	0.11±0.06	0.22±0.08	0.19±0.08	0.20±0.11
SMOEF									
HC	0.18±0.01	0.19±0.01	0.19±0.01	0.26±0.04	0.26±0.03	0.26±0.01	0.18±0.02	0.19±0.02	0.20±0.01
T2DM	0.21±0.004#	0.21±0.01#	0.22±0.03	0.25±0.01	0.24±0.01	0.24±0.01	0.20±0.01	0.21±0.01#	0.20±0.02

Statistically significant between HC and T2DM, * for SMBF, $p < 0.05$; # for SMOEF, $p < 0.05$

SMBF skeletal muscle blood flow, *SMOEF* skeletal muscle oxygen extraction fraction, *SOL* soleus muscle, *GAS* gastrocnemius muscle, *TA* tibialis anterior muscle, *HC* healthy control, *T2DM* type 2 diabetes mellitus

Table 3 Function and strain characteristics

	T2DM	HC	<i>p</i> value
EDV	16.71±3.90	15.96±5.28	NS
ESV	5.62±1.99	5.19±2.52	NS
SV	11.09±2.63	10.77±3.69	NS
CO	1.36±0.31	1.22±0.52	NS
EF (%)	66.80±7.81	67.50±7.83	NS
MyoMass_diast	15.13±4.22	14.62±2.59	NS
MyoMass_syst	20.06±4.82	19.07±3.19	NS
LGE	(–)	(–)	
Radial PS (%)	23.71±14.07	26.37±11.79	NS
Circumferential PS (%)	–15.12±5.48	–16.01±3.05	NS
Longitudinal PS (%)	–9.55±2.77	–13.59±1.97	<0.05
Radial PSSR (1/s)	2.49±1.50	2.46±1.63	NS
Circumferential PSSR (1/s)	–1.67±0.67	–1.36±0.48	NS
Longitudinal PSSR (1/s)	–1.00±0.31	–1.51±0.38	<0.05
Radial PDSR (1/s)	–3.19±2.18	–3.31±1.47	NS
Circumferential PDSR(1/s)	1.72±0.75	1.82±0.39	NS
Longitudinal PDSR (1/s)	0.91±0.20	1.36±0.23	<0.05
Peak torsion (°)	4.01±1.10	6.04±2.95	NS
Peak torsion rate (°/s)	140.13±69.77	132.82±61.16	NS

EDV end-diastolic volume index, *ESV* end-systolic volume index, *SV* stroke volume, *CO* cardiac output, *EF* ejection fraction, *LGE* late gadolinium enhancement, *PS* global peak strain, *PSSR* global peak systolic strain rate, *PDSR* global peak diastolic strain rate

Discussion

In the present study, from all of the MR characteristics of the skeletal muscle and heart, only the longitudinal PSSR were negatively correlated with the SMBF reserves when the skeletal muscles were blocked by a cuff compression. Namely, the absolute values of longitudinal PSSR decreased, and the SMBF reserve in all of the muscle decreased. It is sparse in the previous studies to investigate the relationship between the impairment of skeletal muscle and heart by

radiology in T2DM. One study by Scheuermann-Freestone et al. [20] found that the T2DM patients with apparently normal cardiac function had impaired myocardial and skeletal muscle energy metabolism related to changes in circulating metabolic substrates. But other studies mainly observed the relationship between the derangements in the skeletal muscle and heart dysfunction in the heart failure [8], myocardial infarction [21] and older adults [22], and the values in predicting the major cardiovascular events [23]. Therefore, this study initially reported the image relationship between the microcirculation impairment in skeletal muscle and the myocardial deformation in T2DM.

There are three reasons to explain why only the longitudinal PSSR, in this study, was observed negative correlation with the SMBF reserve. First of all, the pathophysiological studies helped understanding the impairment between skeletal muscle and heart in T2DM. Extensive studies have found that the T2DM is characterized by insulin resistance and elevated plasma glucose concentrations [24], with the skeletal muscle as the major site of glucose uptake and then resulted that the mitochondrial dysfunction and microcirculation dysfunction were the etiology of type 2 diabetes [25], following the myocardium and skeletal muscle damaged. Secondly, previous studies and this study found that the SMBF reserves were the most sensitive parameters, compared to the absolute SMBF and SMOEF values and SMOEF reserves, to detect the impairment of the microcirculation of skeletal muscle in diabetes. This might be resulted from the following reasons: the impaired capillary structure, the impaired capillary response for stimulus [6, 26] and the impaired lower limb skeletal muscle oxidative capacity [27]. In addition, for the SMOEF reserves, although the SOL in human and monkey was proven to mainly compose by slow oxidative type I fibers, which has a higher capillary density and therefore a higher blood volume than fast-twitch glycolytic type II fibers (GAS and TA) [28, 29], the SMOEF reserves were unable to differentiate the impaired in SOL, GAS and TA in T2DM monkeys (Table 2, Fig. 2) and diabetic patients

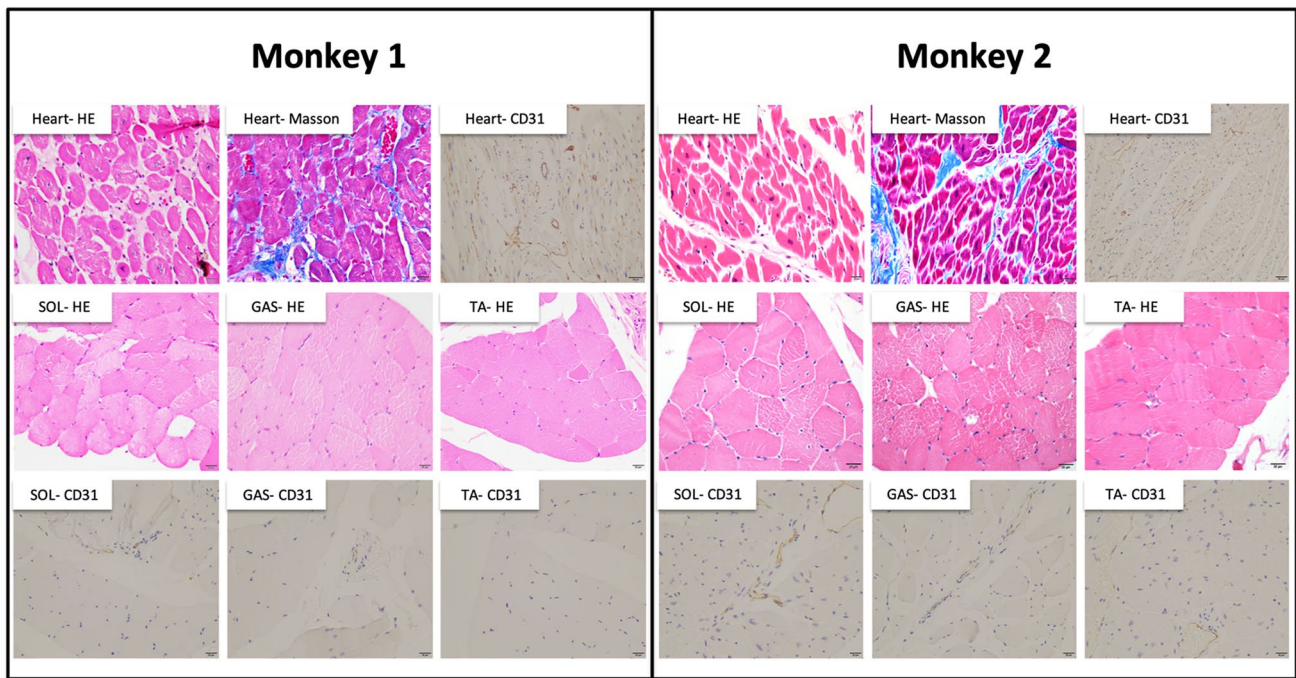


Fig. 3 Histology from two T2DM monkeys. The changed myocardium and skeletal muscle confirmed by HE staining, Masson staining and CD31 staining ($\times 400$)

[15]. Thirdly, the cardiac function and myocardial deformation characteristics of T2DM patients were manifested as the circumferential and longitudinal strains and strain rates decreased [10, 12, 18]. Previous studies found that the longitudinal myocardial fibers were predominantly located in the sub-endocardium, and this wall layer was most susceptible to microvascular ischemia; thus, the changes can lead to a reduction in longitudinal LV mechanics in T2DM, even in an early stage [10, 30]. And LV longitudinal myocardial systolic dysfunction (LVSD) was suggested to be the first marker of a preclinical form of DM-related cardiac dysfunction detected with the echocardiography strain analysis [31, 32]. In this study, we investigated that the longitudinal strain or strain rate, no matter systolic or diastolic, was the major myocardial dysfunction. Therefore, the findings in this study suggest that the impairment of skeletal muscle and heart occurs early in the pathophysiology of T2DM and the myocardial function associated with the microcirculation in skeletal muscle.

However, our study has several limitations. Firstly, the sample size is small. The time-consuming screening makes the number of the spontaneous; T2DM rhesus monkeys were rare. 3 to 4 years were needed generally to confirm the diabetic condition of the monkeys. Further, human studies with a large sample size are warranted. In another, the rare T2DM monkey model led to the limited pathology tissue; thus, it is impossible to quantify the relationship between MRI and pathology. Secondly, the temporal resolution (~ 4 min) for the SMOEF

measurement and the signal-to-noise ratio of cardiac MRI perfusion images and T1 mapping sequences is needed to improve to get more important information in the further studies [19].

In conclusion, this study firstly found that the impaired skeletal muscle and cardiac dysfunction occurred in an early stage of the T2DM with a negative correlation existed in the myocardial longitudinal PSSR and the SMBF reserves. These findings suggested that paying the same attention about the impairment of the heart and skeletal muscle in T2DM is helpful for the early diagnosis and prognosis evaluation.

Funding This study was funded by the National Natural Science Foundation of China (Grant Numbers 81520108014, 81771800, 81829003) and the State's Key Project of Research and Development Plan of China (2016YFA0201402).

Compliance with ethical standards

Conflict of interest The authors declare that they have no conflict of interest.

Ethical standard statement All applicable international, national, and/or institutional guidelines for the care and use of animals were followed. The study was been approved by the Institutional Animal Care and Use Committee of Sichuan PriMed Group Co., Ltd and Sichuan University.

Informed consent For this type of study, formal consent is not required.

References

1. Strain WD, Paldanius PM (2018) Diabetes, cardiovascular disease and the microcirculation. *Cardiovasc Diabetol* 17(1):57. <https://doi.org/10.1186/s12933-018-0703-2>
2. Nathan DM (2015) Diabetes: advances in diagnosis and treatment. *JAMA* 314(10):1052–1062. <https://doi.org/10.1001/jama.2015.9536>
3. Bigagli E, Lodovici M (2019) Circulating oxidative stress biomarkers in clinical studies on type 2 diabetes and its complications. *Oxidative Med Cell Longev* 2019:5953685. <https://doi.org/10.1155/2019/5953685>
4. Baltzis D, Eleftheriadou I, Veves A (2014) Pathogenesis and treatment of impaired wound healing in diabetes mellitus: new insights. *Adv Ther* 31(8):817–836. <https://doi.org/10.1007/s12325-014-0140-x>
5. Nichols GA, Gullion CM, Koro CE, Ephross SA, Brown JB (2004) The incidence of congestive heart failure in type 2 diabetes: an update. *Diabetes Care* 27(8):1879–1884. <https://doi.org/10.2337/diacare.27.8.1879>
6. Zaccardi F, Webb DR, Yates T, Davies MJ (2016) Pathophysiology of type 1 and type 2 diabetes mellitus: a 90-year perspective. *Postgrad Med J* 92(1084):63–69. <https://doi.org/10.1136/postgradmedj-2015-133281>
7. Piepoli MF, Crisafulli A (2014) Pathophysiology of human heart failure: importance of skeletal muscle myopathy and reflexes. *Exp Physiol* 99(4):609–615. <https://doi.org/10.1113/expphysiol.2013.074310>
8. Hirai DM, Copp SW, Holdsworth CT et al (2014) Skeletal muscle microvascular oxygenation dynamics in heart failure: exercise training and nitric oxide-mediated function. *Am J Physiol Heart Circ Physiol* 306(5):H690–H698. <https://doi.org/10.1152/ajpheart.00901.2013>
9. Lavine KJ, Sierra OL (2017) Skeletal muscle inflammation and atrophy in heart failure. *Heart Fail Rev* 22(2):179–189. <https://doi.org/10.1007/s10741-016-9593-0>
10. Liu X, Yang ZG, Gao Y et al (2018) Left ventricular subclinical myocardial dysfunction in uncomplicated type 2 diabetes mellitus is associated with impaired myocardial perfusion: a contrast-enhanced cardiovascular magnetic resonance study. *Cardiovasc Diabetol* 17(1):139. <https://doi.org/10.1186/s12933-018-0782-0>
11. Qian C, Gong L, Yang Z et al (2015) Diastolic dysfunction in spontaneous type 2 diabetes rhesus monkeys: a study using echocardiography and magnetic resonance imaging. *BMC Cardiovasc Disord* 15:59. <https://doi.org/10.1186/s12872-015-0046-9>
12. Zhu T, Zeng W, Chen Y et al (2018) 2D/3D CMR tissue tracking versus CMR tagging in the assessment of spontaneous T2DM rhesus monkeys with isolated diastolic dysfunction. *BMC Med Imaging* 18(1):47. <https://doi.org/10.1186/s12880-018-0288-y>
13. Zheng J, An H, Coggan AR et al (2014) Noncontrast skeletal muscle oximetry. *Magn Reson Med* 71(1):318–325. <https://doi.org/10.1002/mrm.24669>
14. Zheng J, Hastings MK, Muccigross D et al (2015) Non-contrast MRI perfusion angiogram in diabetic feet. *Eur Radiol* 25(1):99–105. <https://doi.org/10.1007/s00330-014-3337-0>
15. Zheng J, Hasting MK, Zhang X et al (2014) A pilot study of regional perfusion and oxygenation in calf muscles of individuals with diabetes with a noninvasive measure. *J Vasc Surg* 59(2):419–426. <https://doi.org/10.1016/j.jvs.2013.07.115>
16. Haddad JA, Haddad AN (2018) The past decade in type 2 diabetes and future challenges. *Hormones (Athens, Greece)* 17(4):451–459. <https://doi.org/10.1007/s42000-018-0080-y>
17. Rayner JO, Kalker R, Goebel S et al (2018) Comparative pathogenesis of Asian and African-Lineage Zika virus in Indian Rhesus Macaque's and development of a non-human primate model suitable for the evaluation of new drugs and vaccines. *Viruses*. <https://doi.org/10.3390/v10050229>
18. Zhang Y, Zeng W, Chen W et al (2019) MR extracellular volume mapping and non-contrast T1rho mapping allow early detection of myocardial fibrosis in diabetic monkeys. *Eur Radiol* 29(6):3006–3016. <https://doi.org/10.1007/s00330-018-5950-9>
19. Wang C, Zhang R, Zhang X et al (2016) Noninvasive measurement of lower extremity muscle oxygen extraction fraction under cuff compression paradigm. *J Magn Reson Imaging JMRI* 43(5):1148–1158. <https://doi.org/10.1002/jmri.25074>
20. Scheuermann-Freestone M, Madsen PL, Manners D et al (2003) Abnormal cardiac and skeletal muscle energy metabolism in patients with type 2 diabetes. *Circulation* 107(24):3040–3046. <https://doi.org/10.1161/01.Cir.0000072789.89096.10>
21. Attar R, Wester A, Koul S, Eggert S, Andell P (2019) Peripheral artery disease and outcomes in patients with acute myocardial infarction. *Open Heart* 6(1):e001004. <https://doi.org/10.1136/openhrt-2018-001004>
22. Keng BMH, Gao F, Teo LLY et al (2019) Associations between skeletal muscle and myocardium in aging: a syndrome of “cardio-sarcopenia”? *J Am Geriatr Soc*. <https://doi.org/10.1111/jgs.16132>
23. Morris DR, Skalina TA, Singh TP, Moxon JV, Golledge J (2018) Association of computed tomographic leg muscle characteristics with lower limb and cardiovascular events in patients with peripheral artery disease. *J Am Heart Assoc* 7(20):e009943. <https://doi.org/10.1161/jaha.118.009943>
24. Zheng Y, Ley SH, Hu FB (2018) Global aetiology and epidemiology of type 2 diabetes mellitus and its complications. *Nat Rev Endocrinol* 14(2):88–98. <https://doi.org/10.1038/nrendo.2017.151>
25. Schrauwen-Hinderling VB, Kooi ME, Schrauwen P (2016) Mitochondrial function and diabetes: consequences for skeletal and cardiac muscle metabolism. *Antioxid Redox Signal* 24(1):39–51. <https://doi.org/10.1089/ars.2015.6291>
26. Lindner JR (2018) Cause or effect? Microvascular dysfunction in insulin-resistant states. *Circ Cardiovasc Imaging* 11(4):e007725. <https://doi.org/10.1161/circimaging.118.007725>
27. Leermakers PA, Gosker HR (2016) Skeletal muscle mitophagy in chronic disease: implications for muscle oxidative capacity? *Curr Opin Clin Nutr Metab Care* 19(6):427–433. <https://doi.org/10.1097/mco.0000000000000319>
28. Schulte AC, Aschwanden M, Bilecen D (2008) Calf muscles at blood oxygen level-dependent MR imaging: aging effects at postocclusive reactive hyperemia. *Radiology* 247(2):482–489. <https://doi.org/10.1148/radiol.2472070828>
29. Fitts RH, Bodine SC, Romatowski JG, Widrick JJ (1985) Velocity, force, power, and Ca²⁺ sensitivity of fast and slow monkey skeletal muscle fibers. *J Appl Physiol* 59(5):1776–1787. <https://doi.org/10.1152/jappl.1998.84.5.1776>
30. Kalam K, Otahal P, Marwick TH (2014) Prognostic implications of global LV dysfunction: a systematic review and meta-analysis of global longitudinal strain and ejection fraction. *Heart (Br Card Soc)* 100(21):1673–1680. <https://doi.org/10.1136/heartjnl-2014-305538>
31. Mochizuki Y, Tanaka H, Matsumoto K et al (2017) Impact of left ventricular longitudinal functional mechanics on the progression of diastolic function in diabetes mellitus. *Int J Cardiovasc Imaging* 33(12):1905–1914. <https://doi.org/10.1007/s10554-017-1198-8>
32. Hatani Y, Tanaka H, Mochizuki Y et al (2019) Association of body fat mass with left ventricular longitudinal myocardial systolic function in type 2 diabetes mellitus. *J Cardiol*. <https://doi.org/10.1016/j.jcc.2019.07.013>

Publisher's Note Springer Nature remains neutral with regard to jurisdictional claims in published maps and institutional affiliations.